optica

Photonic chip-based resonant supercontinuum via pulse-driven Kerr microresonator solitons

MILES H. ANDERSON,[1] ROMAIN BOUCHAND,[1] JUNQIU LIU,[1] WENLE WENG,[1] EWELINA OBRZUD,[2,3] TOBIAS HERR,[4] AND TOBIAS J. KIPPENBERG[1,*]

[1] Institute of Physics, Swiss Federal Institute of Technology (EPFL), Lausanne, Switzerland
[2] Swiss Center for Electronics and Microtechnology (CSEM), Time and Frequency, Neuchâtel, Switzerland
[3] Department of Astronomy & Geneva Observatory/PlanetS, University of Geneva, Versoix, Switzerland
[4] Center for Free-Electron Laser Science (CFEL), Deutsches Elektronen-Synchrotron (DESY), Hamburg, Germany
*Corresponding author: tobias.kippenberg@epfl.ch

Received 20 July 2020; revised 10 November 2020; accepted 15 April 2021 (Doc. ID 403302); published 24 May 2021

Supercontinuum generation and soliton microcomb formation both represent key techniques for the formation of coherent, ultrabroad optical frequency combs, enabling the RF-to-optical link. Coherent supercontinuum generation typically relies on ultrashort pulses with kilowatt peak power as a source, and so are often restricted to repetition rates less than 1 GHz. Soliton microcombs, conversely, have an optical conversion efficiency that is best at ultrahigh repetition rates such as 1 THz. Neither technique easily approaches the microwave domain, i.e., 10 s of GHz, while maintaining an ultrawide spectrum. Here, we bridge the efficiency gap between the two approaches in the form of resonant supercontinuum generation by driving a dispersion-engineered photonic-chip-based microresonator with picosecond pulses of the order of 1-W peak power. We generate a smooth 2200-line soliton-based comb at an electronically detectable 28 GHz repetition rate. Importantly, we observe that solitons exist in a weakly bound state with the input pulse where frequency noise transfer from the input pulses is suppressed even for offset frequencies 100 times lower than the linear cavity decay rate. This transfer can be reduced even further by driving the cavity asynchronously, ensuring the frequency comb stays coherent even for optical lines very far from the pump center.

https://doi.org/10.1364/OPTICA.403302

1. INTRODUCTION

Supercontinuum generation (SCG) or "white light" generation [1,2] is one of the most dramatic nonlinear phenomena discovered [3,4]. It refers to a process where high-intensity optical pulses are converted into coherent octave-spanning spectra by propagation through a dispersion-engineered waveguide, fiber, or material [Fig. 1(a)]. Following the demonstration of dramatic broadening in optical fibers [3], it enabled the self-referencing of optical frequency combs, establishing the RF-to-optical link [5,6]. Since then, the process has been well studied in photonic crystal fibers [7,8], owing to their capacity for dispersion engineering.

SCG is based on a combination of nonlinear phenomena including soliton fission, dispersive wave formation, and the Raman self-frequency shift [9]. Commonly, to generate a supercontinuum that is coherent as well as having ultrahigh bandwidth, ultrashort pulses (~100 fs) with high peak powers (>1 kW) are needed so that the pulse undergoes a process known as soliton fission under conditions of anomalous dispersion [9,10], as opposed to incoherent modulation instability [11] (MI). Dispersive wave emission (alternatively, soliton Cherenkov radiation [12]) simultaneously serves to extend the spectrum towards other spectral regions far from the pump [13]. More coherent SCG can be done under normal dispersion dominated by self-phase modulation (SPM); however, this generally hinders the achievable bandwidth [8]. To obtain a broadband spectrum, SCG has most often required the input of mode-locked laser systems operating at repetition rates of <1 GHz so as to provide high peak power. Although photonic-chip-based waveguides with a high material nonlinearity have reduced required pulse energies by an order of magnitude, and have allowed lithographic dispersion engineering [14–17], synthesis of octave spanning spectra with line spacing >10 GHz has remained challenging. Accessing this regime has been achieved using SCG driven with electro-optic (EO) frequency combs [18–21], providing ultrabroad frequency comb formation at repetition rates of 10–30 GHz, although multiple stages of amplification and pulse compression were required to replicate the same pulse duration and peak powers available from mode-locked lasers.

An alternative technique for the generation of coherent frequency comb spectra is Kerr comb generation [22], i.e., soliton microcombs. Kerr comb generation uses the resonant buildup of a continuous-wave laser to generate a frequency comb via parametric frequency conversion and the formation of dissipative Kerr solitons (DKSs) [23]. These DKSs exhibit a rich landscape of dynamical states, such as breathing [24,25], chaos [26], and bound states [27]. In contrast to SCG, DKSs circulate indefinitely,

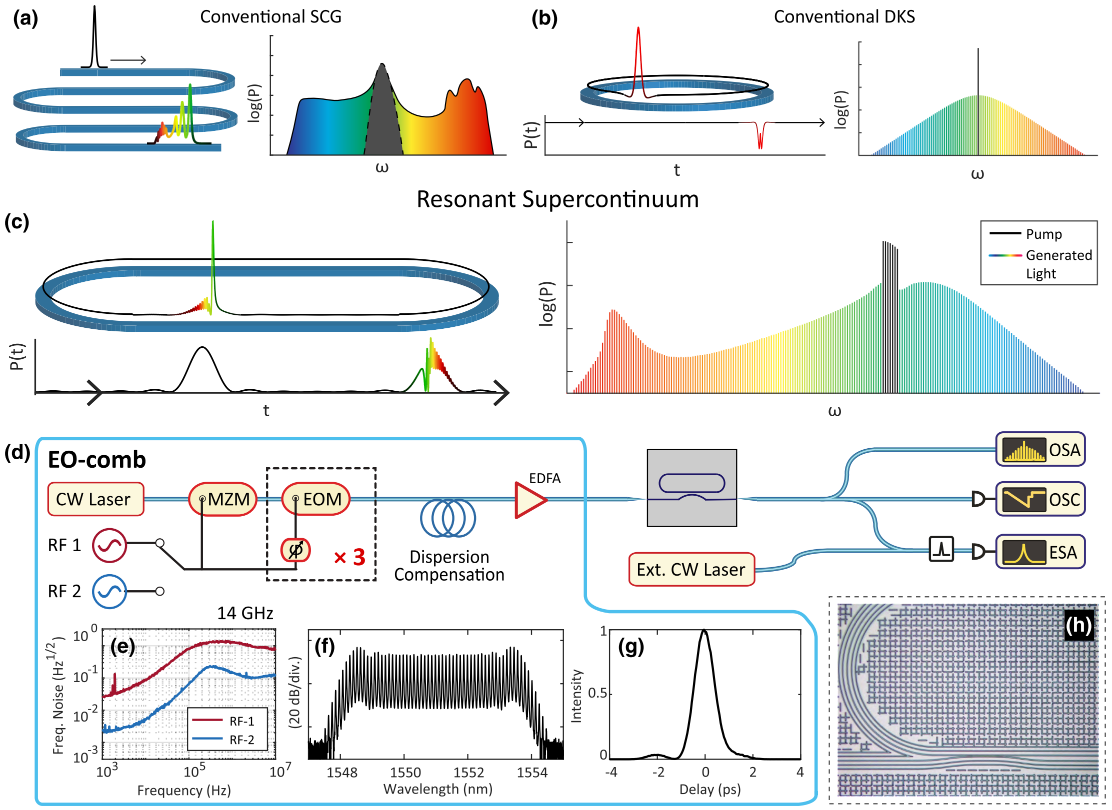

Fig. 1. Resonant supercontinuum generation using a dispersion engineered Si_3N_4 photonic chip. (a)–(c) Principles of broadband frequency comb generation compared. (d) Experimental setup. MZM, Mach–Zehnder modulator; EOM, electro-optic modulator; EDFA, erbium-doped fiber amplifier; ESA, electronic spectrum analyzer; OSA, optical spectrum analyzer; OSC, oscilloscope. The input pulse train is coupled into and out of the microresonator chip via lensed fibers. (e) Frequency noise of the two RF signal generators at 14 GHz. (f) Spectrum of the 14-GHz EO comb before amplification. (g) Retrieved FROG measurement of the optimum pulse duration. (h) Microscope image of part of the microresonator, depicting the coupling section.

relying on a double balance of nonlinearity and dispersion as well as parametric gain and dissipation [28]. The cavity enhances the pump field, dramatically reducing the input power threshold for soliton formation. Yet, the process itself has a conversion efficiency that reduces with decreasing repetition rate owing to the reduced overlap of the DKS and the background pump [29] [Fig. 1(b)]. As a consequence, octave-spanning soliton microcombs to date have been synthesized with 1 THz line spacing only [30,31], and it has proven challenging to synthesize spectra with 10–50 GHz repetition rate with either SCG or microcomb formation. However, a growing number of applications benefit from coherent supercontinua with line spacing in the microwave domain that can be easily detected and processed by electronics, such as optical frequency division [32] and Raman spectral imaging [33]. Such widely spaced comb spectra are resolvable in diffraction-based spectrometers for astrocombs [34–36], and are highly appropriate as sources for massively parallel wavelength-division multiplexing [37,38]. They can also remove the ambiguity in the identification of individual comb lines.

In this work, we demonstrate *resonant* SCG, a synthesis between conventional SCG and soliton microcombs [Fig. 1(c)]. By supplying a microresonator with a pulsed input, we take equal advantage of the resonant enhancement offered by the cavity, as well as the higher peak input powers and conversion efficiency allowed by pulses as compared to CW [39]. Prior experiments on SCG with "feedback" have been carried out in the regime of strong broadening and high loss each roundtrip, i.e., low cavity finesse [40,41]. This work of what we term as "resonant" supercontinuum takes place in the regime of ultrahigh microcavity finesse (>100) where loss and nonlinear processes occur over hundreds of roundtrips. In both cases, the microresonator physics can be modeled using the generalized nonlinear Schrödinger equation (GNLSE) piece-wise with the resonator-to-bus waveguide coupler term forming the cavity [42,43]. In this limit of high finesse, the dynamics may in turn be modeled using a single mean-field model, the *Lugiato–Lefever equation* (LLE), and hence can be considered to be equivalent to pulse-driven Kerr microresonator physics.

Where recent works on pulse-driven Kerr cavities for DKS generation have focused on single soliton generation with high conversion efficiency over a narrower optical band [44], and peak-power enhancement [43], the use of dispersion-optimized photonic waveguides to generate a spectrum with an enhanced bandwidth and flatness has not yet been demonstrated with this method. Here, we make use of the low-loss photonic Si_3N_4 resonator platform [45]. By promoting low dispersion with a strong third-order component, we generate DKS states exhibiting strong Cherenkov radiation, bound to the driving pulse. In the frequency domain, this forms a flattened, broadband spectrum close to 2/3 of an octave wide, using only pulses that are 10 times longer in duration, and with peak power three orders of magnitude lower, than in typical Si_3N_4-based SCG [21,46], and with an electronically detectable repetition rate of 28 GHz. Compared to contemporary CW-driven soliton microcombs, this spectrum is five times broader than those with similar line spacing [47], and seven times more spectrally dense than those with a similar bandwidth [48].

We further investigate, numerically and experimentally, the nature of the bonding between the generated DKSs and the driving pulse [49], particularly the *nonlinear* filtering [50] of noise transfer this weak bonding gives rise to. This nonlinear filtering is found, remarkably, to combat noise multiplication, a known drawback of EO-comb-driven SCG, where frequency noise on the input pulse repetition rate is transferred and multiplied over the generated optical lines, destroying their coherence [19,51]. We find a way to optimize this filtering, in both simulations and experiment.

2. RESULTS

The chip-based Si_3N_4 microresonator used for this experiment [section depicted in Fig. 1(h)], has a free spectral range (FSR) of 27.88 GHz and a loaded linewidth in the telecom band of $\kappa = 2\pi.110$ MHz (most probable value [52]). The waveguide dimensions have been selected to give a comparatively low dispersion [47] of $\beta_2 = -11\ \mathrm{fs}^2/\mathrm{mm}$. The pulse train incident on this chip is synthesized using cascaded EO modulation, intensity modulation, and dispersion compensation [53,54] [Fig. 1(d)], providing pulses with a minimum duration of 1 ps, at a repetition rate $f'_{eo} = 13.94$ GHz. In this way, the microresonator is subharmonically pumped every two round trips [35], and only every second comb line interacts with the cavity modes at an effective $f_{eo} = 2f'_{eo}$. This decreases the conversion efficiency by a factor of two, but reduces the requirements on the microwave transmission system. A tunable RF signal generator supplies f_{eo}, and we keep two alternative RF sources—with relatively high (RF-1) and low (RF-2) phase-noise—to observe how their frequency noise is transferred to the resonant supercontinuum. Further details are found in Supplement 1 (Section 1).

DKS states are generated on the input pulses by sweeping their carrier frequency ω_p from the blue- to the red-detuned side of the cavity resonance ω_0, to the region of cavity bistability [23], such that the detuning $\delta\omega = \omega_0 - \omega_p > 0$. Before a DKS can be formed stably, the difference between the repetition rate of the pulse train f_{eo} and the cavity FSR has to be matched to within a "locking range." Inside this range, the generated soliton becomes locked to the driving pulse [44] (or modulated background [55]), so that the comb $f_{rep} = f_{eo}$. A simulated example of this is depicted in Fig. 2(a). In this experiment, the locking range is ~30–50 kHz.

The measured output spectrum of the microresonator during single-state DKS operation is presented in Fig. 2(c), generated at two input powers: the minimum required to form a DKS, and a higher power generating the most energetic spectrum for this work. They both exist at the maximum accessible cavity detuning $\delta\omega$, where the spectral bandwidth of the DKS scales as $\Omega_S \propto \sqrt{P_0}$ [56,57], hence the dramatic broadening of the spectra. The first, least energetic soliton has a 3-dB bandwidth of 9.5 THz, and an estimated pulse duration of 55 fs based on a sech^2 fit. The energy of a soliton scales the same way [29]; hence, this first DKS has the highest conversion efficiency from the input comb to generated lines of 8%. The high-energy DKS measurably spans 64 THz or 600 nm, accounting for 2300 measurable lines (1400 in 10 dB), and has a conversion efficiency of 2.8%. This is the highest line count for a single-state DKS, with a bandwidth exceeding the C + L bands, to our knowledge. Simulations shown in Figs. 2(a) and 2(b) replicating the measured spectrum predict a distorted DKS due to the strong dispersive wave emission, and having a duration of ~24 fs. The spectrum is strongly enhanced on the long-wavelength side due to the prominent third-order dispersion of the waveguide, forming a dispersive wave at 1957 nm, combined with the soliton Raman self-frequency shift, which has shifted the spectral center from the pump at 1558 nm towards 1590 nm [58,59].

Importantly, no fast-tuning methods [60] were required to form DKS. Piezo-tuning was sufficient, suggesting a practical absence of cavity thermal relaxation, which has complicated stable soliton generation in the past [31,61]. The number of DKS ranged from one to three. The effective average power required to generate these single-soliton states ranges from 18 to 180 mW. The corresponding pulse energies range from 0.6 to 6 pJ, and we estimate the peak powers to be from 0.6 to 6 W based on the frequency-resolved optical gating (FROG) measurement of the pulse profile [Fig. 1(g)]. These values indicate a high efficiency compared to the results obtained by CW-driving the same microresonator. In that case, parametric oscillation was reached at only 115 mW of on-chip pump power. Beyond that, *only* a soliton crystal state [62] comprising 185 individual DKSs was able to be formed at 345 mW, and beyond that, only chaotic states were observed. These CW-driving results can be found in Supplement 1 (Section 2).

In terms of SCG, the lack of broadening undergone by the pump pulse spectrum as it travels the 5 mm length of the bus waveguide is put into stark contrast with the large bandwidth of the DKSs generated due the enhancement of the pump pulse inside the resonator (also of length 5 mm). Such resonant enhancement has allowed the pump pulse to reach an effective soliton order $N \approx 40$ as it continually circulates *inside* the resonator, allowing it to undergo the MI phase seen in Fig. 2(a) at zero detuning. Only the dissipative, bistable nature of the Kerr cavity allows a single soliton to be isolated at a large detuning, a process unavailable in single-pass supercontinuum. By this reasoning, we identify the experiment as resonant supercontinuum. Further analysis on this is in Supplement 1 (Section 7).

A. Coherence Properties

Figure 2(d) shows the repetition rate beatnote of the DKS *excluding* the EO-comb spectrum. The beatnote corresponds exactly to two times the RF source frequency, and with a 1-Hz limited linewidth demonstrates high repetition rate stability. For measuring the optical coherence of the comb, optical heterodyne measurements are taken against increasing values of μ, the comb line index from the center pump, from 1550 nm to the outer edge at 1908 nm plotted in Figs. 2(e)–2(g). Figure 2(e) shows a narrow heterodyne beatnote at the edge of the EO comb. As comb lines become farther away from the center, their linewidths quickly broaden, as shown in Fig. 2(f), where we plot heterodyne beatnotes up to a range of 70 nm from the comb center. This noise multiplication continues to the long-wavelength edge of the comb, where the heterodyne beatnote with a narrow-linewidth 1908-nm laser is plotted in Fig. 2(g). Here, the linewidth has expanded to around 7.5 MHz according to Gaussian fitting.

When we switch our RF signal generator from RF-1 to the lower noise source RF-2, and measure the heterodyne comb beatnotes at the same wavelengths in Figs. 2(f) and 2(g) (two example measurements given in (f) and one in (g), we find that linewidths are decisively more narrow. The linewidth at 1908 nm in particular

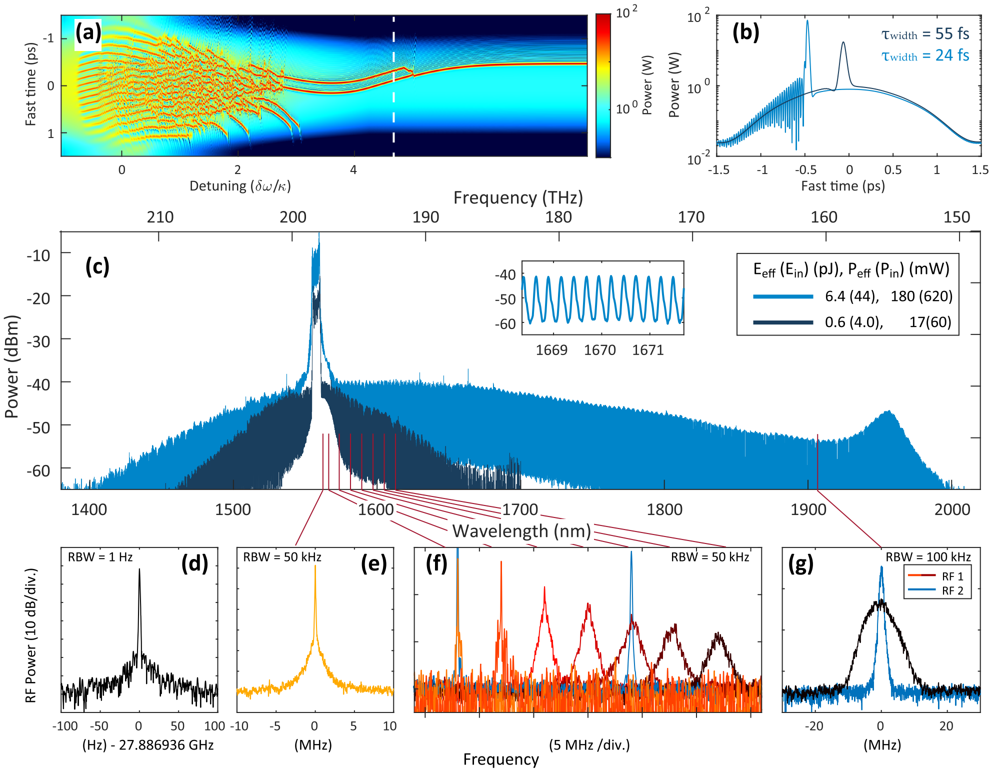

Fig. 2. Resonant supercontinuum generation and coherence. (a) Simulation of the time-domain intracavity field of the pulse-driven microresonator during a scan over resonance, for a total time of $t = 800\,\kappa^{-1}$. The scan is halted at detuning $\delta\omega = 5\,\kappa$ (white-dashed line). The pulse background has a repetition rate mismatch $d = -50$ kHz to compensate for the offset DKS group velocity. (b) Simulation time-domain slice of a dissipative soliton upon the pulse input at two power levels corresponding to the experiment in (c). (c) Generated spectrum at maximum detuning. Lowest energy soliton with minimum pulsed power required in dark blue. Fully formed spectrum using higher power in light blue. Inset: comb lines resolved by the OSA. Input power and pulse energy noted as *effective* power coupled to the microresonator (total power incident on chip), taking into account chip insertion loss and ×2 pulse inefficiency. (d) Soliton repetition rate beatnote. (e) Beatnote at the 12th line at the edge of the EO comb. (f) Beatnotes of μth comb line, measured between the pump and 1620 nm, from left to right $\mu = -45, -88, -132, -175, -217, -259, -300$ (horizontally offset by 4 MHz for clarity). (g) Beatnote at 1908 nm ($\mu = -1300$). Legend applies across (f) and (g).

has reduced by almost a factor of 10, down to 900 kHz. This difference in coherence at the wings of the spectrum, using different EO-comb RF sources, confirms to us that this is the result of RF noise multiplication, imposed on the comb spacing through the locking between the input pulse and the DKS. However, as shown in Supplement 1 (Section 3), when we form a conventional supercontinuum using an EO comb driven by the same RF sources, we can detect the beatnote at 1908 nm *only* when RF-2 is used, not RF-1. This indicates the presence of an additional filtering effect possessed only by the DKS.

3. NOISE TRANSFER ANALYSIS

If one were to assume that the generated soliton is *perfectly* locked to the input pulse, we would expect the optical frequency noise of each soliton comb line to be coupled to the RF noise on the coupled pulse repetition rate $f_{\text{eo}} = 28$ GHz, such that $S_{\delta\nu}^{(\mu)}(f) = \mu^2 S_f^{(\text{rf})}(f)$, with relative comb index μ (assuming other sources of laser noise are small by comparison). However, this is not the case for a DKS. The frequency-noise multiplication transfer function can be found in numerical simulations based on the LLE [63] with parameters similar to that of a typical Si_3N_4 resonator, where instead of a normally CW-driving term, we use a pulsed input $F(\phi)$ (where ϕ is the spatial coordinate of the cavity) similar in duration to that used in the experiment. It is also slightly positively chirped, in line with our experimental EO-comb compression stage (see Supplement 1, Section 1), giving a negative phase curvature on the pulse [64]. Frequency noise equivalent to a uniform power-spectral density of $S_f^{(\text{rf})}(f) = 1.0\ \text{Hz}^2/\text{Hz}$ is applied to the input pulse over a long period of "slow time" ($t > 4{,}000\,\kappa^{-1}$), and the corresponding jitter of the soliton is captured. For this first simulation, we have set f_{eo}, the input pulse repetition rate, to be equal to the FSR for fully synchronous driving.

The simulation results are shown in Fig. 3. In the time domain [shown in Figs. 3(a) and 3(b)], the generated soliton is located at its "trapping point" at ∼0.6 ps at the trailing edge of the pulse [49], but under these synchronous and symmetrical pulse conditions, it may equally find itself at −0.6 ps on the leading edge. As it is trapped, or locked, to the background input pulse, it inherits jitter and gradually walks back and forth in the "fast time" domain. The noise applied to the input pulse itself during this one example, and its corresponding walk in the time domain, is plotted in Fig. 3(c).

The corresponding frequency domain results are shown in Figs. 3(d) and 3(e). Figure 3(e) in particular is obtained by taking the Fourier transform over both dimensions of the optical field in Fig. 3(b), therefore plotting the power spectral densities on the y

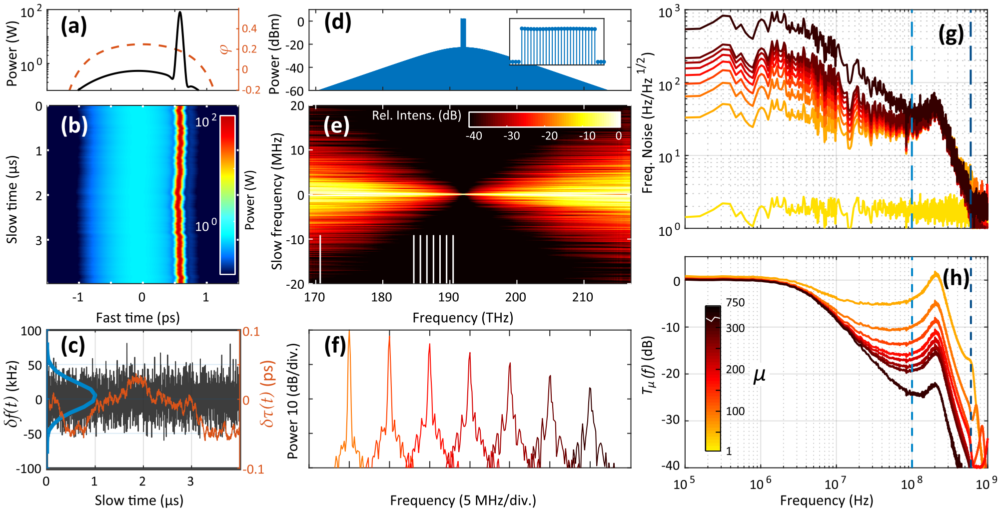

Fig. 3. Simulation of noise multiplication and nonlinear filtering, based on the Lugiato–Lefever equation. (a) Intracavity field at time t. Instantaneous phase of the background pulse as dashed line. (b) Slow time versus fast time graph of intracavity field. (c) Frequency noise (gray, histogram in blue), and corresponding absolute timing jitter (orange), imposed on the input pulse over the period of the simulation. (d) Output spectrum, with inset showing input spectrum. (e) Slow frequency versus fast frequency graph of the long-term frequency comb, with columns normalized to peak. White marks indicate comb lines depicted in (g) and (h). (f) Individual noisy comb lines selected from (d), with same comb mode μ as in the experiment [Fig. 2(f)]. (g) Frequency noise spectra and (h) corresponding RF-noise transfer functions for individual comb lines marked in (e), including a comb line far from center ($\mu = -750$). Dashed lines indicate the linear cavity bandwidth (light blue), and cavity detuning (dark blue). Traces are averaged from eight simulations for clarity.

axis of each individual comb line along the x axis—a simulated heterodyne beatnote (normalized to peak). As is evident, the linewidth of each comb line widens considerably as it becomes farther from the comb center. In Fig. 3(f), individual beatnotes corresponding to the same comb line measurements shown in Fig. 2(f) show good qualitative agreement.

The profile of this frequency noise transfer to individual comb lines is given in Figs. 3(g) and 3(h), where we plot their frequency noise spectra and corresponding normalized transfer functions $T^{(\mu)}(f) = S_{\delta\nu}^{(\mu)}/(\mu^2 S_f^{(\mathrm{rf})})$, respectively. As expected for low offset frequencies, noise power is fully multiplied by μ^2, fulfilling the requirement for the soliton to be locked to the input pulse over the long term. Strikingly, however, above some cutoff frequency $f_c \approx 3$ MHz, the transfer of noise power drops significantly at a slope of -20 dB/decade, showing how the soliton is able to "ignore" the fast background motion of the input pulse despite being locked to it over the long term. Interestingly, this cutoff frequency is of the order of 100 times lower than the linear cavity bandwidth for this simulated $\mathrm{Si_3N_4}$ cavity, of 100 MHz, demonstrating that this filtering is born of the nonlinear DKS regime, as has been observed in $\mathrm{MgF_2}$ crystalline microresonators [55]. Beyond this cutoff point, the transfer function begins to be dominated by the response of the cavity [65], where we see a resonance located after the cavity bandwidth at κ, and a further strong cutoff at the cavity detuning at $\delta\omega = 2\pi \cdot 600$ MHz. The exact nature of these resonances is beyond the scope of this work, though the simulated traces presented here are in excellent qualitative agreement with the numerical and experimental results presented in an independent and concurrent work by Brasch *et al.* [50], where the full linear and nonlinear response is investigated in detail.

A. Optimization of Nonlinear Filtering

Returning attention to the experimental heterodyne beatnote measurement at 1908 nm, we have observed an interesting effect when the driving repetition f_{eo} is varied. Figure 4(a) shows the 1908-nm beatnote as f_{eo} is swept from the minimum to the maximum of the soliton locking range (0 kHz defined as the minimum). The linewidth appears to narrow, reaching a minimum at the upper edge of the locking range, in this case 50 kHz. To characterize this narrowing phenomenon, we measured the frequency noise spectrum of this beatnote using in-phase/quadrature analysis [66] as f_{eo} is varied across the locking range, which is shown in Fig. 4(b). Also overlaid is $2\mu\sqrt{S_f^{(\mathrm{rf1})}}$, where $S_f^{(\mathrm{rf1})}$ here is the independently measured frequency noise spectrum of the signal generator RF-1 at 14 GHz, with comb line $\mu = 1300$, (and factor of two from the half rep-rate driving up-scaled to 28 GHz). We further plot the corresponding experimental transfer functions $T^{(\mu)}(f)$, as before, in Fig. 4(c). As shown, the frequency noise level of the 1908-nm beatnote very closely follows the multiplied RF noise until a certain cutoff frequency, which varies from a maximum of 2 MHz reducing to ~500 kHz at the edge of the locking range. In excellent qualitative agreement with the simulation results in Fig. 3, the value of this corner frequency is of the order of 100 times less than the linear cavity bandwidth, of 110 MHz, experimentally confirming the presence of nonlinear filtering.

We next carry out numerical simulations to analyze the f_{eo}-dependent nonlinear filtering behavior. We apply a mismatch between the input pulse train repetition rate and the native repetition rate of the soliton ($d = f_{\mathrm{eo}} - \mathrm{FSR}$). Figure 4(e) shows the same type of result as Fig. 3(e), only now for a DKS comb for four different values of d (manifesting as the gradient in the comb line centers) between -50 and 50 kHz. The effect on the comb linewidth broadening is dramatic. The simulated comb line for $\mu = -1300$ as d is varied between 0 and 50 kHz (maximum of the locking range) is displayed in Fig. 4(f), showing excellent qualitative agreement with the experimental observation in Fig. 4(a).

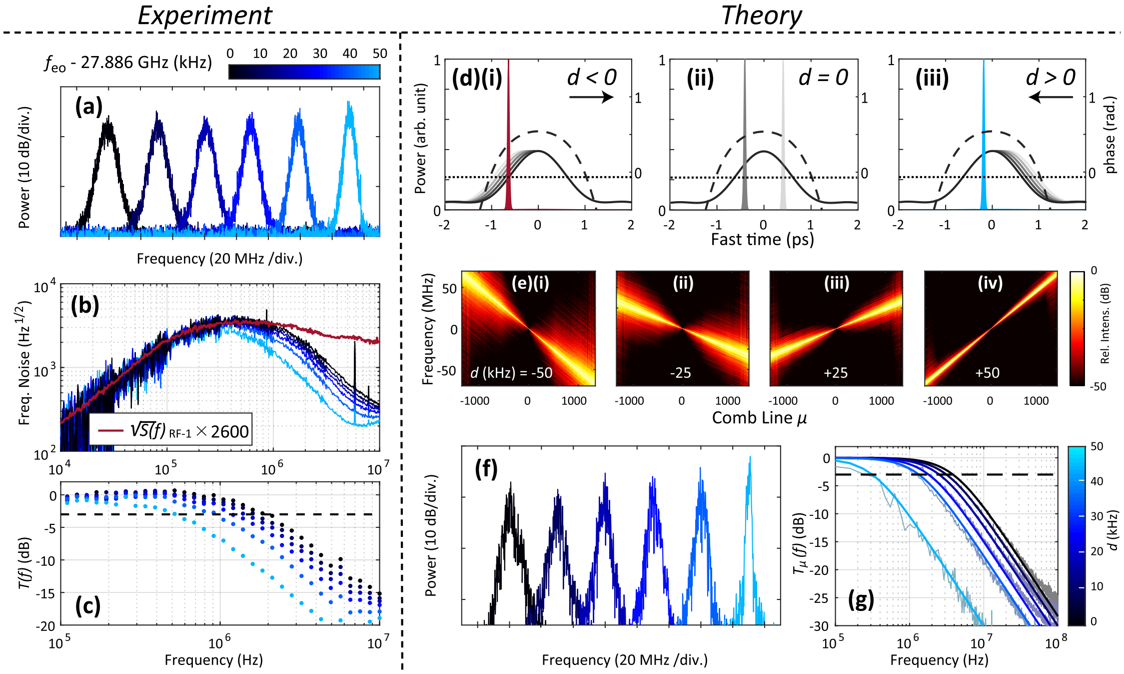

Fig. 4. Optimization of soliton-based nonlinear filtering via asynchronous driving: experiment and simulation. (a) Experimental DKS heterodyne beatnote at 1908 nm ($\mu = -1300$) as f_{eo} is varied over a range of 50 kHz. Beatnotes horizontally offset each by 30 MHz for clarity. (b) Corresponding measured frequency noise, plotted with the multiplied frequency noise of RF-1. (c) Experimental transfer function based on (b), with 3-dB level marked with dashed line. (d) i–iii Conceptual soliton trapping locations on a chirped pulse background under different values of de-synchronized driving d. Arrow indicates background repetition-rate mismatch, with pulse phase profile (dashed) and F_C (dotted). (e) i-iv Simulated slow versus fast frequency graphs for different values of de-synchronization d. (f) Slice of the $\mu = -1300$ beatnote (1908 nm) in slow frequency for d from 0 to 50 kHz (blue). (g) Simulated noise transfer functions for d from 0 to 50 kHz. Low-pass fit profile in colored line, original results in gray.

Our experimental and simulation results reveal that as the repetition rate mismatch d changes, the "trapping" location of the DKS on the driving pulse, as well as the local trapping gradient can be significantly different. Previous studies have demonstrated that solitons can acquire a non-zero drift across the cavity space due to the presence of a gradient on the background driving field. Specifically, for a purely phase-modulated background, the soliton will become attracted to the *peak* of the phase profile [67]. Conversely, for pure amplitude variation, a soliton will become attracted to the *edge* of the pulse at some critical intensity level F_C approximately equivalent to the lowest pump power that can sustain a soliton at high detuning [49,68] (defined in Supplement 1, Section 4). In our experiment, the driving field is essentially a mixture of both amplitude modulation (pulse driving) and phase modulation (additional chirping). As a result, the soliton is drawn towards an *intermediate* trapping location between the intensity-based trap at the edge of the pulse, and the phase-based trap at the peak. This trapping point will be modified by d, which acts as an effective force [69]. For a DKS to continue to sustain itself, it must follow the pulse at its own shifted repetition rate, so that

$$2\pi d + \frac{\partial \phi_S}{\partial t} = 0, \tag{1}$$

where ϕ_S is the angular coordinate of the soliton inside the resonator. If d is non-zero, the soliton must move to a different location to acquire a shifted repetition rate, due the gradient in background phase and/or intensity [67,68]. Figure 4(d) illustrates these situations from (i) to (iii), where $d < 0$, $d = 0$, and $d > 0$. The soliton is initially positioned on the left, leading edge of the pulse. In Fig. 4(d-i), the mismatch d and the intensity-based trapping force have combined to shift the soliton to the very left edge of the pulse. In (d-ii), the soliton is located at its intermediate trapping point, which is symmetrical with the pulse. In (d-iii), the mismatch d adds to the phase-based trapping force, causing the soliton to move closer to the peak. The observed change in the noise transfer bandwidth with varied d can be understood intuitively as being due to the local trapping gradient [68] that gradually decreases from the edge of the pulse to the center. Analogous to atoms/particles trapped by optical potential wells [70], a DKS trapped at a location closer to the input pulse center is subject to a shallower potential gradient, thus becoming more "free running" and less affected by the noise contained in the driving field. For Fig. 4(e-i) where the soliton is being "pulled" on the edge of the pulse, the broadening is maximized. For (e-iv), where the soliton is instead being "pushed" near the peak of the pulse, it has almost reduced to zero. The reduced noise transfer effect is well reproduced by our simulation, as shown in Fig. 4(g). As d increases, the DKS gets closer to the pulse center. Consequently, the cutoff frequency of the noise transfer function decreases, showing remarkable qualitative agreement with the experimental measurement in Fig. 4(c).

The hypothetical carrier–envelope offset f_{ceo} beatnote measurement of this microcomb would carry a further factor of ~5 increase in the frequency noise level. To mitigate this, a future pulse-driven experiment may involve the use of a shaped "flattop" pulse with a shallow depression in the center. Such a centrally inverted profile would allow the DKS to find itself trapped in a shallow basin *inside* the pulse envelope transferring minimal input pulse jitter, yet maintaining very long-term stability. See Supplement 1 (Section 5) for this outlook simulation.

4. SUMMARY

Using the nonlinear, dispersion-engineered Si_3N_4 microresonator platform, we have generated a smooth, resonant supercontinuum based on dissipative soliton formation, comprising over 2000 comb teeth. By exploiting the resonant enhancement of the high-Q cavity, such a spectrum was generated with pulses 1–6 pJ in energy, >1 ps in duration, and of the order of single-Watt peak power. For future integration, the current EO-comb input could be replaced by an alternative provider of gigahertz rate, picosecond pulses, such as chip-based silicon or other semiconductor-based mode-locked lasers [71,72]. Further tailoring of the dispersion landscape [30,73] and replacing the straight-waveguide coupling section with an adiabatic or curved coupling section [74,75] will improve the generation and extraction of the short-wavelength side of the spectrum. This way, the soliton comb bandwidth can be increased from two-thirds of an octave to a full octave, enabling $f-2f$ self-referencing. This work further invites a full exploration of the parameter space for input pulse chirp and flatness parameters to find further optimization of the frequency noise transfer, allowing the use of higher-noise voltage-controlled oscillators for locking the input pulse repetition rate. Overall, this work demonstrates a new chip-based technique for direct access to broadband spectra at microwave repetition rates using a pulsed input, without the use of interleaving, or additional EO modulation after the fact. Importantly, it can provide a way of balancing the fundamental efficiency restrictions between conventional SCG and dissipative soliton microcombs.

Funding. Defense Advanced Research Projects Agency (DARPA) (D18AC00032), Defense Sciences Office (DSO); Schweizerischer Nationalfonds zur Förderung der Wissenschaftlichen Forschung (192293, 176563); Air Force Office of Scientific Research (FA9550-19-1-0250); EU H2020 Marie Skłodowska-Curie Actions (753749).

Acknowledgment. W.W. acknowledges support from the EU's H2020 research and innovation programme under Marie Skłodowska-Curie IF grant agreement No. 753749 (SOLISYNTH). T.H. acknowledges support through the Helmholtz Young Investigator Group VH-NG-1404 and the European Research Council (ERC) under the European Union's Horizon 2020 research and innovation program (853564). M.H.A. performed the experiment with the assistance of R.B., E.O., and T.H. The sample microresonator was fabricated by J.L. M.H.A. conducted the numerical analysis. The paper was prepared by M.H.A. with the assistance of R.B., W.W., T.J.K., and T.H. T.J.K. supervised the project.

Disclosures. The authors declare no conflicts of interest.

Data Availability. The code and data that support the plots within this paper are available at [76]. All other data and findings of this study are available from the corresponding author upon reasonable request.

Supplemental document. See Supplement 1 for supporting content.

REFERENCES

1. R. R. Alfano and S. L. Shapiro, "Observation of self-phase modulation and small-scale filaments in crystals and glasses," Phys. Rev. Lett. **24**, 592–594 (1970).
2. M. Bellini and T. W. Hänsch, "Phase-locked white-light continuum pulses: toward a universal optical frequency-comb synthesizer," Opt. Lett. **25**, 1049–1051 (2000).
3. J. K. Ranka, R. S. Windeler, and A. J. Stentz, "Visible continuum generation in air–silica microstructure optical fibers with anomalous dispersion at 800 nm," Opt. Lett. **25**, 25–27 (2000).
4. T. A. Birks, W. J. Wadsworth, and P. St.J. Russell, "Supercontinuum generation in tapered fibers," Opt. Lett. **25**, 1415–1417 (2000).
5. D. J. Jones, S. A. Diddams, J. K. Ranka, A. Stentz, R. S. Windeler, J. L. Hall, and S. T. Cundiff, "Carrier-envelope phase control of femtosecond mode-locked lasers and direct optical frequency synthesis," Science **288**, 635–639 (2000).
6. T. Udem, R. Holzwarth, and T. W. Hänsch, "Optical frequency metrology," Nature **416**, 233–237 (2002).
7. P. St.J. Russell, "Photonic-crystal fibers," J. Lightwave Technol. **24**, 4729–4749 (2006).
8. J. M. Dudley, G. Genty, and S. Coen, "Supercontinuum generation in photonic crystal fiber," Rev. Mod. Phys. **78**, 1135–1184 (2006).
9. D. V. Skryabin and A. V. Gorbach, "*Colloquium*: looking at a soliton through the prism of optical supercontinuum," Rev. Mod. Phys. **82**, 1287–1299 (2010).
10. J. Herrmann, U. Griebner, N. Zhavoronkov, A. Husakou, D. Nickel, J. C. Knight, W. J. Wadsworth, P. St.J. Russell, and G. Korn, "Experimental evidence for supercontinuum generation by fission of higher-order solitons in photonic fibers," Phys. Rev. Lett. **88**, 173901 (2002).
11. M. Nakazawa, K. Tamura, H. Kubota, and E. Yoshida, "Coherence degradation in the process of supercontinuum generation in an optical fiber," Opt. Fiber Technol. **4**, 215–223 (1998).
12. N. Akhmediev and M. Karlsson, "Cherenkov radiation emitted by solitons in optical fibers," Phys. Rev. A **51**, 2602–2607 (1995).
13. K. M. Hilligsøe, H. N. Paulsen, J. Thøgersen, S. R. Keiding, and J. J. Larsen, "Initial steps of supercontinuum generation in photonic crystal fibers," J. Opt. Soc. Am. B **20**, 1887–1893 (2003).
14. D.-I. Yeom, E. C. Mägi, M. R. E. Lamont, M. A. F. Roelens, L. Fu, and B. J. Eggleton, "Low-threshold supercontinuum generation in highly nonlinear chalcogenide nanowires," Opt. Lett. **33**, 660–662 (2008).
15. R. Halir, Y. Okawachi, J. S. Levy, M. A. Foster, M. Lipson, and A. L. Gaeta, "Ultrabroadband supercontinuum generation in a CMOS-compatible platform," Opt. Lett. **37**, 1685–1687 (2012).
16. F. Leo, S.-P. Gorza, J. Safioui, P. Kockaert, S. Coen, U. Dave, B. Kuyken, and G. Roelkens, "Dispersive wave emission and supercontinuum generation in a silicon wire waveguide pumped around the 1550 nm telecommunication wavelength," Opt. Lett. **39**, 3623–3626 (2014).
17. H. Guo, C. Herkommer, A. Billat, D. Grassani, C. Zhang, M. H. P. Pfeiffer, W. Weng, C.-S. Brès, and T. J. Kippenberg, "Mid-infrared frequency comb via coherent dispersive wave generation in silicon nitride nanophotonic waveguides," Nat. Photonics **12**, 330–335 (2018).
18. R. Wu, V. Torres-Company, D. E. Leaird, and A. M. Weiner, "Supercontinuum-based 10-GHz flat-topped optical frequency comb generation," Opt. Express **21**, 6045–6052 (2013).
19. K. Beha, D. C. Cole, P. Del'Haye, A. Coillet, S. A. Diddams, and S. B. Papp, "Electronic synthesis of light," Optica **4**, 406–411 (2017).
20. E. Obrzud, M. Rainer, A. Harutyunyan, B. Chazelas, M. Cecconi, A. Ghedina, E. Molinari, S. Kundermann, S. Lecomte, F. Pepe, F. Wildi, F. Bouchy, and T. Herr, "Broadband near-infrared astronomical spectrometer calibration and on-sky validation with an electro-optic laser frequency comb," Opt. Express **26**, 34830–34841 (2018).
21. D. R. Carlson, D. D. Hickstein, W. Zhang, A. J. Metcalf, F. Quinlan, S. A. Diddams, and S. B. Papp, "Ultrafast electro-optic light with subcycle control," Science **361**, 1358–1363 (2018).
22. T. J. Kippenberg, A. L. Gaeta, M. Lipson, and M. L. Gorodetsky, "Dissipative Kerr solitons in optical microresonators," Science **361**, eaan8083 (2018).
23. T. Herr, V. Brasch, J. D. Jost, C. Y. Wang, N. M. Kondratiev, M. L. Gorodetsky, and T. J. Kippenberg, "Temporal solitons in optical microresonators," Nat. Photonics **8**, 145–152 (2014).
24. F. Leo, L. Gelens, P. Emplit, M. Haelterman, and S. Coen, "Dynamics of one-dimensional Kerr cavity solitons," Opt. Express **21**, 9180–9191 (2013).
25. E. Lucas, M. Karpov, H. Guo, M. L. Gorodetsky, and T. J. Kippenberg, "Breathing dissipative solitons in optical microresonators," Nat. Commun. **8**, 736 (2017).
26. M. Anderson, F. Leo, S. Coen, M. Erkintalo, and S. G. Murdoch, "Observations of spatiotemporal instabilities of temporal cavity solitons," Optica **3**, 1071–1074 (2016).
27. Y. Wang, F. Leo, J. Fatome, M. Erkintalo, S. G. Murdoch, and S. Coen, "Universal mechanism for the binding of temporal cavity solitons," Optica **4**, 855–863 (2017).
28. N. Akhmediev and A. Ankiewicz, eds., *Dissipative Solitons: From Optics to Biology and Medicine*, Lecture Notes in Physics (Springer, 2008).

29. C. Bao, L. Zhang, A. Matsko, Y. Yan, Z. Zhao, G. Xie, A. M. Agarwal, L. C. Kimerling, J. Michel, L. Maleki, and A. E. Willner, "Nonlinear conversion efficiency in Kerr frequency comb generation," Opt. Lett. **39**, 6126 (2014).
30. M. H. P. Pfeiffer, C. Herkommer, J. Liu, H. Guo, M. Karpov, E. Lucas, M. Zervas, and T. J. Kippenberg, "Octave-spanning dissipative Kerr soliton frequency combs in Si_3N_4 microresonators," Optica **4**, 684–691 (2017).
31. Q. Li, T. C. Briles, D. A. Westly, T. E. Drake, J. R. Stone, B. R. Ilic, S. A. Diddams, S. B. Papp, and K. Srinivasan, "Stably accessing octave-spanning microresonator frequency combs in the soliton regime," Optica **4**, 193–203 (2017).
32. X. Xie, R. Bouchand, D. Nicolodi, M. Giunta, W. Hänsel, M. Lezius, A. Joshi, S. Datta, C. Alexandre, M. Lours, P.-A. Tremblin, G. Santarelli, R. Holzwarth, and Y. Le Coq, "Photonic microwave signals with zeptosecond-level absolute timing noise," Nat. Photonics **11**, 44–47 (2017).
33. T. Ideguchi, S. Holzner, B. Bernhardt, G. Guelachvili, N. Picqué, and T. W. Hänsch, "Coherent Raman spectro-imaging with laser frequency combs," Nature **502**, 355–358 (2013).
34. M. T. Murphy, T. Udem, R. Holzwarth, A. Sizmann, L. Pasquini, C. Araujo-Hauck, H. Dekker, S. D'Odorico, M. Fischer, T. W. Hänsch, and A. Manescau, "High-precision wavelength calibration of astronomical spectrographs with laser frequency combs," Mon. Not. R. Astron. Soc. **380**, 839–847 (2007).
35. E. Obrzud, M. Rainer, A. Harutyunyan, M. H. Anderson, J. Liu, M. Geiselmann, B. Chazelas, S. Kundermann, S. Lecomte, M. Cecconi, A. Ghedina, E. Molinari, F. Pepe, F. Wildi, F. Bouchy, T. J. Kippenberg, and T. Herr, "A microphotonic astrocomb," Nat. Photonics **13**, 31–35 (2019).
36. M.-G. Suh, X. Yi, Y.-H. Lai, S. Leifer, I. S. Grudinin, G. Vasisht, E. C. Martin, M. P. Fitzgerald, G. Doppmann, J. Wang, D. Mawet, S. B. Papp, S. A. Diddams, C. Beichman, and K. Vahala, "Searching for exoplanets using a microresonator astrocomb," Nat. Photonics **13**, 25–30 (2019).
37. P. Marin-Palomo, J. N. Kemal, M. Karpov, A. Kordts, J. Pfeifle, M. H. P. Pfeiffer, P. Trocha, S. Wolf, V. Brasch, M. H. Anderson, R. Rosenberger, K. Vijayan, W. Freude, T. J. Kippenberg, and C. Koos, "Microresonator-based solitons for massively parallel coherent optical communications," Nature **546**, 274–279 (2017).
38. H. Hu, F. D. Ros, M. Pu, F. Ye, K. Ingerslev, E. P. da Silva, M. Nooruzzaman, Y. Amma, Y. Sasaki, T. Mizuno, Y. Miyamoto, L. Ottaviano, E. Semenova, P. Guan, D. Zibar, M. Galili, K. Yvind, T. Morioka, and L. K. Oxenløwe, "Single-source chip-based frequency comb enabling extreme parallel data transmission," Nat. Photonics **12**, 469–473 (2018).
39. M. Malinowski, A. Rao, P. Delfyett, and S. Fathpour, "Optical frequency comb generation by pulsed pumping," APL Photon. **2**, 066101 (2017).
40. P. Groß, N. Haarlammert, M. Kues, T. Walbaum, and C. Fallnich, "Effects of optical feedback on femtosecond supercontinuum generation," Opt. Fiber Technol. **18**, 290–303 (2012).
41. P. M. Moselund, M. H. Frosz, C. L. Thomsen, and O. Bang, "Back-seeding of higher order gain processes in picosecond supercontinuum generation," Opt. Express **16**, 11954–11968 (2008).
42. M. Anderson, Y. Wang, F. Leo, S. Coen, M. Erkintalo, and S. G. Murdoch, "Coexistence of multiple nonlinear states in a tristable passive Kerr resonator," Phys. Rev. X **7**, 031031 (2017).
43. N. Lilienfein, C. Hofer, M. Högner, T. Saule, M. Trubetskov, V. Pervak, E. Fill, C. Riek, A. Leitenstorfer, J. Limpert, F. Krausz, and I. Pupeza, "Temporal solitons in free-space femtosecond enhancement cavities," Nat. Photonics **13**, 214–218 (2019).
44. E. Obrzud, S. Lecomte, and T. Herr, "Temporal solitons in microresonators driven by optical pulses," Nat. Photonics **11**, 600–607 (2017).
45. Y. Okawachi, M. R. E. Lamont, K. Luke, D. O. Carvalho, M. Yu, M. Lipson, and A. L. Gaeta, "Bandwidth shaping of microresonator-based frequency combs via dispersion engineering," Opt. Lett. **39**, 3535–3538 (2014).
46. Y. Okawachi, M. Yu, J. Cardenas, X. Ji, A. Klenner, M. Lipson, and A. L. Gaeta, "Carrier envelope offset detection via simultaneous supercontinuum and second-harmonic generation in a silicon nitride waveguide," Opt. Lett. **43**, 4627–4630 (2018).
47. J. Liu, E. Lucas, A. S. Raja, J. He, J. Riemensberger, R. N. Wang, M. Karpov, H. Guo, R. Bouchand, and T. J. Kippenberg, "Photonic microwave generation in the X- and K-band using integrated soliton microcombs," Nat. Photonics **14**, 486–491 (2020).
48. V. Brasch, M. Geiselmann, T. Herr, G. Lihachev, M. H. P. Pfeiffer, M. L. Gorodetsky, and T. J. Kippenberg, "Photonic chip-based optical frequency comb using soliton Cherenkov radiation," Science **351**, 357–360 (2016).
49. I. Hendry, W. Chen, Y. Wang, B. Garbin, J. Javaloyes, G.-L. Oppo, S. Coen, S. G. Murdoch, and M. Erkintalo, "Spontaneous symmetry breaking and trapping of temporal Kerr cavity solitons by pulsed or amplitude-modulated driving fields," Phys. Rev. A **97**, 053834 (2018).
50. V. Brasch, E. Obrzud, S. Lecomte, and T. Herr, "Nonlinear filtering of an optical pulse train using dissipative Kerr solitons," Optica **6**, 1386–1393 (2019).
51. A. Ishizawa, T. Nishikawa, A. Mizutori, H. Takara, A. Takada, T. Sogawa, and M. Koga, "Phase-noise characteristics of a 25-GHz-spaced optical frequency comb based on a phase- and intensity-modulated laser," Opt. Express **21**, 29186–29194 (2013).
52. J. Liu, A. S. Raja, M. Karpov, B. Ghadiani, M. H. P. Pfeiffer, B. Du, N. J. Engelsen, H. Guo, M. Zervas, and T. J. Kippenberg, "Ultralow-power chip-based soliton microcombs for photonic integration," Optica **5**, 1347–1353 (2018).
53. T. Kobayashi, H. Yao, K. Amano, Y. Fukushima, A. Morimoto, and T. Sueta, "Optical pulse compression using high-frequency electrooptic phase modulation," IEEE J. Quantum Electron. **24**, 382–387 (1988).
54. M. Fujiwara, M. Teshima, J. Kani, H. Suzuki, N. Takachio, and K. Iwatsuki, "Optical carrier supply module using flattened optical multicarrier generation based on sinusoidal amplitude and phase hybrid modulation," J. Lightwave Technol. **21**, 2705–2714 (2003).
55. W. Weng, E. Lucas, G. Lihachev, V. E. Lobanov, H. Guo, M. L. Gorodetsky, and T. J. Kippenberg, "Spectral purification of microwave signals with disciplined dissipative Kerr solitons," Phys. Rev. Lett. **122**, 013902 (2019).
56. S. Coen and M. Erkintalo, "Universal scaling laws of Kerr frequency combs," Opt. Lett. **38**, 1790–1792 (2013).
57. E. Lucas, H. Guo, J. D. Jost, M. Karpov, and T. J. Kippenberg, "Detuning-dependent properties and dispersion-induced instabilities of temporal dissipative Kerr solitons in optical microresonators," Phys. Rev. A **95**, 043822 (2017).
58. M. Karpov, H. Guo, A. Kordts, V. Brasch, M. H. Pfeiffer, M. Zervas, M. Geiselmann, and T. J. Kippenberg, "Raman self-frequency shift of dissipative Kerr solitons in an optical microresonator," Phys. Rev. Lett. **116**, 103902 (2016).
59. X. Yi, Q.-F. Yang, K. Y. Yang, and K. Vahala, "Theory and measurement of the soliton self-frequency shift and efficiency in optical microcavities," Opt. Lett. **41**, 3419–3422 (2016).
60. E. S. Lamb, D. R. Carlson, D. D. Hickstein, J. R. Stone, S. A. Diddams, and S. B. Papp, "Optical-frequency measurements with a Kerr microcomb and photonic-chip supercontinuum," Phys. Rev. Appl. **9**, 024030 (2018).
61. V. Brasch, M. Geiselmann, M. H. P. Pfeiffer, and T. J. Kippenberg, "Bringing short-lived dissipative Kerr soliton states in microresonators into a steady state," Opt. Express **24**, 29312–29320 (2016).
62. M. Karpov, M. H. P. Pfeiffer, H. Guo, W. Weng, J. Liu, and T. J. Kippenberg, "Dynamics of soliton crystals in optical microresonators," Nat. Phys. **15**, 1071–1077 (2019).
63. L. A. Lugiato and R. Lefever, "Spatial dissipative structures in passive optical systems," Phys. Rev. Lett. **58**, 2209–2211 (1987).
64. G. Agrawal, "Pulse propagation in fibers," in *Nonlinear Fiber Optics*, 5th ed., Optics and Photonics (Academic, 2013), Chap. 2, pp. 27–56.
65. H. Guo, M. Karpov, E. Lucas, A. Kordts, M. H. P. Pfeiffer, V. Brasch, G. Lihachev, V. E. Lobanov, M. L. Gorodetsky, and T. J. Kippenberg, "Universal dynamics and deterministic switching of dissipative Kerr solitons in optical microresonators," Nat. Phys. **13**, 94–102 (2017).
66. M. Schiemangk, S. Spießberger, A. Wicht, G. Erbert, G. Tränkle, and A. Peters, "Accurate frequency noise measurement of free-running lasers," Appl. Opt. **53**, 7138–7143 (2014).
67. J. K. Jang, M. Erkintalo, S. Coen, and S. G. Murdoch, "Temporal tweezing of light through the trapping and manipulation of temporal cavity solitons," Nat. Commun. **6**, 7370 (2015).
68. I. Hendry, B. Garbin, S. G. Murdoch, S. Coen, and M. Erkintalo, "Impact of desynchronization and drift on soliton-based Kerr frequency combs in the presence of pulsed driving fields," Phys. Rev. A **100**, 023829 (2019).
69. J. Javaloyes, P. Camelin, M. Marconi, and M. Giudici, "Dynamics of localized structures in systems with broken parity symmetry," Phys. Rev. Lett. **116**, 133901 (2016).

70. W. D. Phillips, “Nobel lecture: laser cooling and trapping of neutral atoms,” Rev. Mod. Phys. **70**, 721–741 (1998).
71. M. L. Davenport, S. Liu, and J. E. Bowers, “Integrated heterogeneous silicon/III-V mode-locked lasers,” Photon. Res. **6**, 468–478 (2018).
72. P. J. Delfyett, A. Klee, K. Bagnell, P. Juodawlkis, J. Plant, and A. Zaman, “Exploring the limits of semiconductor-laser-based optical frequency combs,” Appl. Opt. **58**, D39–D49 (2019).
73. D. T. Spencer, T. Drake, T. C. Briles, J. Stone, L. C. Sinclair, C. Fredrick, Q. Li, D. Westly, B. R. Ilic, A. Bluestone, N. Volet, T. Komljenovic, L. Chang, S. H. Lee, D. Y. Oh, M.-G. Suh, K. Y. Yang, M. H. P. Pfeiffer, T. J. Kippenberg, E. Norberg, L. Theogarajan, K. Vahala, N. R. Newbury, K. Srinivasan, J. E. Bowers, S. A. Diddams, and S. B. Papp, “An optical-frequency synthesizer using integrated photonics,” Nature **557**, 81–85 (2018).
74. G. F. R. Chen, J. R. Ong, T. Y. L. Ang, S. T. Lim, C. E. Png, and D. T. H. Tan, “Broadband silicon-on-insulator directional couplers using a combination of straight and curved waveguide sections,” Sci. Rep. **7**, 7246 (2017).
75. G. Moille, Q. Li, T. C. Briles, S.-P. Yu, T. Drake, X. Lu, A. Rao, D. Westly, S. B. Papp, and K. Srinivasan, “Broadband resonator-waveguide coupling for efficient extraction of octave-spanning microcombs,” Opt. Lett. **44**, 4737–4740 (2019).
76. M. H. Anderson, R. Bouchand, J. Liu, W. Weng, E. Obrzud, T. Herr, and T. J. Kippenberg, “Available data for ’Photonic chip-based resonant supercontinuum via pulse-driven Kerr microresonator solitons’,” Zenodo, 2021, https://doi.org/10.5281/zenodo.4750315